npj | Quantum Materials

www.nature.com/npjquantmats

ARTICLE OPEN

Check for updates

Resonant inelastic X-ray scattering as a probe of $J_{\mathrm{eff}} = 1/2$ state in 3*d* transition-metal oxide

H. Y. Huang[1], A. Singh[1], C. I. Wu[2], J. D. Xie[3], J. Okamoto[1], A. A. Belik[4], E. Kurmaev[5], A. Fujimori[1,6], C. T. Chen[1], S. V. Streltsov[5,7]✉ and D. J. Huang[1,3,8]✉

The state with effective total moment $J_{\mathrm{eff}} = 1/2$ stabilized by the spin-orbit coupling is known to suppress Jahn-Teller distortions and may induce a strong exchange anisotropy. This in turn may lead to the formation of an elusive spin-liquid state in real materials. While recent studies have demonstrated that such a situation can be realized in 3*d* transition-metal compounds such as those based on Co^{2+} and Cu^{2+}, diagnosis of $J_{\mathrm{eff}} = 1/2$ state remains challenging. We show that resonant inelastic X-ray scattering is an effective tool to probe this state and apply it to $CuAl_2O_4$, material where Cu^{2+} ions were previously proposed to be in the $J_{\mathrm{eff}} = 1/2$ state. Our results unambiguously demonstrate that, contrary to previous expectations, a competitive (to $J_{\mathrm{eff}} = 1/2$) Jahn-Teller state realizes in this compound.

npj Quantum Materials (2022)7:33 ; https://doi.org/10.1038/s41535-022-00430-0

INTRODUCTION

Spin-orbit materials, i.e., systems in which physical properties are strongly affected by the spin-orbit coupling (SOC), undoubtedly became one of the central subjects in modern condensed matter physics[1,2]. In particular, it is essential for various topological effects and anisotropic exchange interaction in magnetic materials, which may result, e.g., in a mysterious Kitaev quantum spin liquid[3,4]. Since the SOC constant is large for heavy elements[5], the investigations were initially concentrated on the 4*d* and 5*d* transition-metal compounds such as $\alpha - RuCl_3$ and $(Li,Na)_2IrO_3$[4,6,7]. However, it was very recently shown that more conventional 3*d* oxides also can demonstrate similar behavior with the ground state characterized by an effective moment $J_{\mathrm{eff}} = 1/2$ (New is often well overlooked old.)[8,9].

Indeed, the spin-orbital entangled state can be realized, for example, in the case of Co^{2+} ions having octahedral coordination or Cu^{2+} ions surrounded by a ligand tetrahedron. Intensive ongoing studies of layered honeycomb cobaltites have demonstrated that anisotropic and bond-dependent exchange coupling can be sufficiently strong and may result in an elusive quantum spin liquid state[10–13]. Strong exchange anisotropy was also predicted for Cu^{2+} ions occupying *A* sites in spinels such as $CuAl_2O_4$, if the ground state is characterized by $J_{\mathrm{eff}} = 1/2$[14,15]. However, whether this situation realizes accurate 3*d* materials is an open question.

Resonant inelastic X-ray scattering (RIXS) was shown to be a powerful technique for studying Kitaev materials based on 4*d* and 5*d* transition metals. It can be used both to estimate physical parameters of a system, such as the crystal-field splitting or the SOC constant, and also anomalous magnetic excitation spectra of Kitaev systems, see, e.g.,[16–20]. In the present work we demonstrate that RIXS turns out to be a sensitive probe in the case of 3*d* transition-metal compounds and can discriminate between conventional $S = 1/2$ and spin-orbit $J_{\mathrm{eff}} = 1/2$ states, which may lead to anisotropic exchange interactions. Applying this technique to $CuAl_2O_4$, we show that the vibronic coupling suppresses the formation of the $J_{\mathrm{eff}} = 1/2$ state in this material.

$CuAl_2O_4$ belongs to the *A*-site spinel system, in which the Cu^{2+} ions site at the center of the tetrahedral *A*-sites and the nonmagnetic Al^{3+} ions are located at the center of octahedral *B*-sites. The 3*d* states of tetrahedral Cu^{2+} are split into t_2 and *e* states because of the T_d crystal field of the four oxygen ions, as illustrated in Fig. 1. An atomic t_2^5 configuration is therefore realized with a single hole in the upper t_2 manifold, making $CuAl_2O_4$ a possible candidate of the spin-orbit Mott insulator because the on-site Coulomb interaction amplifies the effect of relativistic SOC[14,15,21]. The t_2 degeneracy can be lifted through the following two channels. In the presence of SOC, the triply degenerate t_2 states are split into states of effective total angular momenta $J_{\mathrm{eff}} = 1/2$ and 3/2 through the approximation of effective orbital angular momentum $L_{\mathrm{eff}} = 1$ for t_2 states. Hence the ground state would be a spin-orbital entangled state in the SOC limit. On the other hand, the degeneracy can be lifted due to the Jahn-Teller distortion, which lowers the T_d symmetry of crystal field, resulting in a spin-half ground state with a quenched orbital angular momentum.

Recent theoretical studies based on first-principles calculations conclude that $CuAl_2O_4$ is a spin-orbital-entangled $J_{\mathrm{eff}} = 1/2$ Mott insulator[14,15]. X-ray and neutron diffraction results also show that the crystal structure of $CuAl_2O_4$ at ambient pressure is in cubic phase without evidence of tetragonal distortion[22]. However, the breakdown of local symmetry induced by Jahn-Teller distortion can not be ruled out. Moreover, the diffraction data have shown a finite site-disorder in $CuAl_2O_4$, where about 30% of Cu^{2+} ions occupy the octahedral sites[23,24]. To unravel the ground state of $CuAl_2O_4$, we used Cu *L*-edge RIXS to investigate the electronic structure as RIXS is an element- and site-selective probe. In combining with multiplet calculations, our RIXS results demonstrate the existence

[1]National Synchrotron Radiation Research Center, Hsinchu 30076, Taiwan. [2]Graduate Program in Science and Technology of Synchrotron Light Source, National Tsing Hua University, Hsinchu 30013, Taiwan. [3]Department of Electrophysics, National Yang Ming Chiao Tung University, Hsinchu 30010, Taiwan. [4]International Center for Materials Nanoarchitectonics (WPI-MANA), National Institute for Materials Science (NIMS), Namiki 1-1, Tsukuba, Ibaraki 305-0044, Japan. [5]Institute of Metal Physics, S. Kovalevskoy Street 18, 620990 Ekaterinburg, Russia. [6]Department of Applied Physics, Waseda University, Shinjuku-ku, Tokyo 169-8555, Japan. [7]Department of theoretical physics and applied mathematics, Ural Federal University, Mira St. 19, 620002 Ekaterinburg, Russia. [8]Department of Physics, National Tsing Hua University, Hsinchu 30013, Taiwan.
✉email: streltsov@imp.uran.ru; djhuang@nsrrc.org.tw

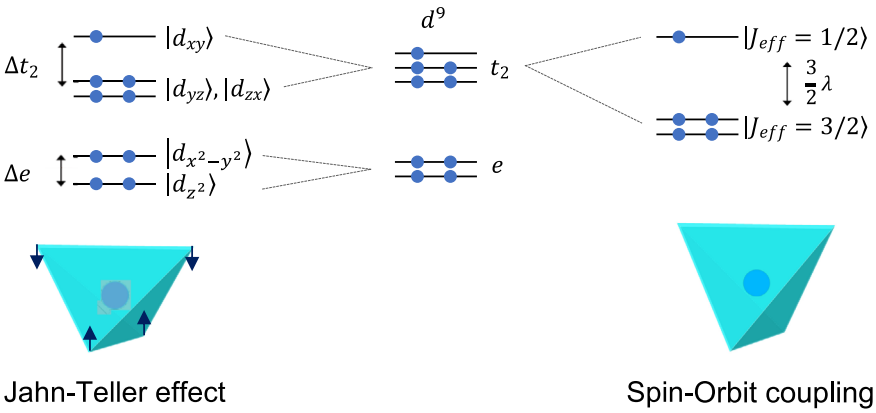

Fig. 1 Schematic illustration on the t_2 splitting of tetrahedral Cu^{2+} due to the Jahn-Teller effect (left) and spin-orbit coupling (right).

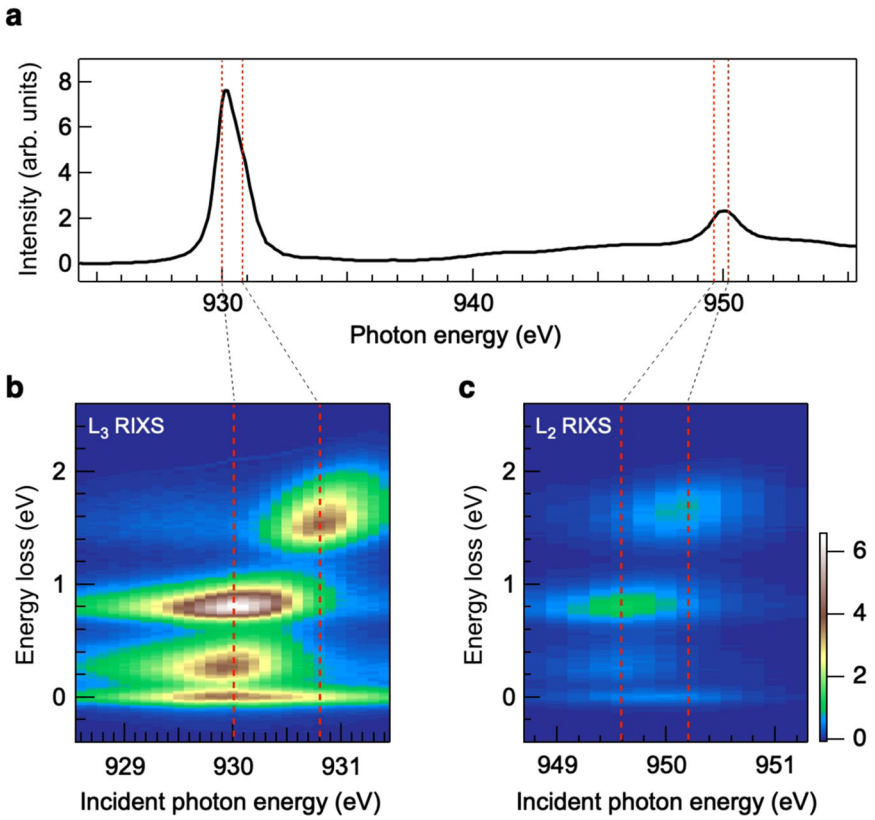

Fig. 2 RIXS intensity distribution maps of $CuAl_2O_4$ in the plane of energy loss vs. incident photon energy. **a** Cu *L*-edge XAS spectrum measured with total electron yield. **b** & **c** RIXS intensity maps measured around Cu L_3 and L_2 edges, respectively. The vertical red dashed lines indicate RIXS features from tetrahedral and octahedral Cu^{2+}, corresponding to the absorption energies of the XAS spectrum shown in (**a**), i.e., 930 & 949.6 eV and 930.8 & 950.2 eV, respectively. All spectra were recorded at room temperature with π-polarized incident X-ray.

of local Jahn-Teller distortion in the tetrahedral sites, in contrast to the scenario of spin-orbital entanglement.

RESULTS

X-ray absorption

L-edge X-ray absorption spectroscopy (XAS) is an effective tool to investigate the SOC in the ground state of transition-metal compounds because it probes the dipole transitions from 2*p* electrons to unoccupied *d* states. If the Cu^{2+} is in the pure $J_{\rm eff} = 1/2$ ground state, the L_2 edge is forbidden due to the dipole selection rule, i.e., the transition from $2p_{1/2}$ to $J_{\rm eff} = 1/2$ is not allowed[25,26]. Figures 2(a) plots Cu *L*-edge XAS of $CuAl_2O_4$. Consistent with recent XAS results of single-crystal $CuAl_2O_4$[22], our data show that the L_3-edge XAS contains two distinct features; they arise from the transition to the unoccupied 3*d* states of tetrahedral and octahedral Cu^{2+}. In addition, we observed non-vanishing Cu L_2-edge XAS intensity, implying the existence of octahedral Cu^{2+} or tetrahedral Cu^{2+} which has a ground state with a Jahn-Teller distortion. Although previous XAS study concluded that the L_2 XAS intensity solely originates from the octahedral Cu^{2+} site[22], the measured XAS can also be explained by the scenario of the coexistence of octahedral Cu^{2+} and tetrahedral Cu^{2+} of a spin-half ground state. In other words, whether $CuAl_2O_4$ is a $J_{\rm eff} = 1/2$ Mott insulator remains an open question. To resolve this issue, we resort to RIXS measurements to

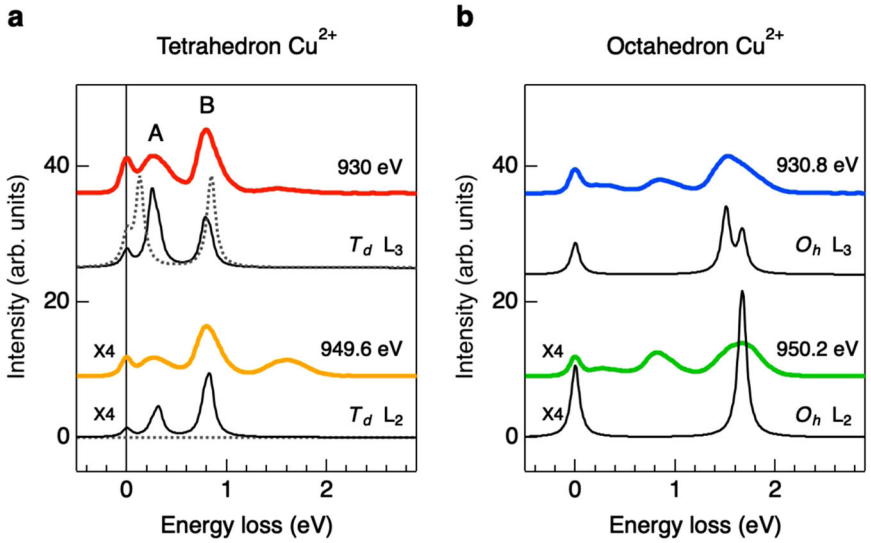

Fig. 3 Cu *L*-edge RIXS spectra recorded at selected incident photon energies in comparison with multiplet calculations. a RIXS spectra measured with the incident photon energies tuned to the resonance of T_d Cu^{2+} compared with calculated RIXS. The solid black lines plot the calculated spectra of T_d Cu^{2+} with the Jahn-Teller distortion; the dashed gray lines are for those in a spin-orbital entangled state. The calculated RIXS intensity of T_d Cu^{2+} in the $J_{eff} = 1/2$ state vanishes. See the main text for the discussion on the origin of peaks A and B. **b** Measured RIXS of O_h Cu^{2+} in comparision with calculations. The solid black lines plot the calculated spectra of O_h Cu^{2+} without a distortion. The incident photon energies E_{in} indicated in (**a**) and (**b**) correspond to the red dashed lines shown in Fig. 2. Both experimental and calculated RIXS spectra of Cu L_2 edge are magnified by a factor of four.

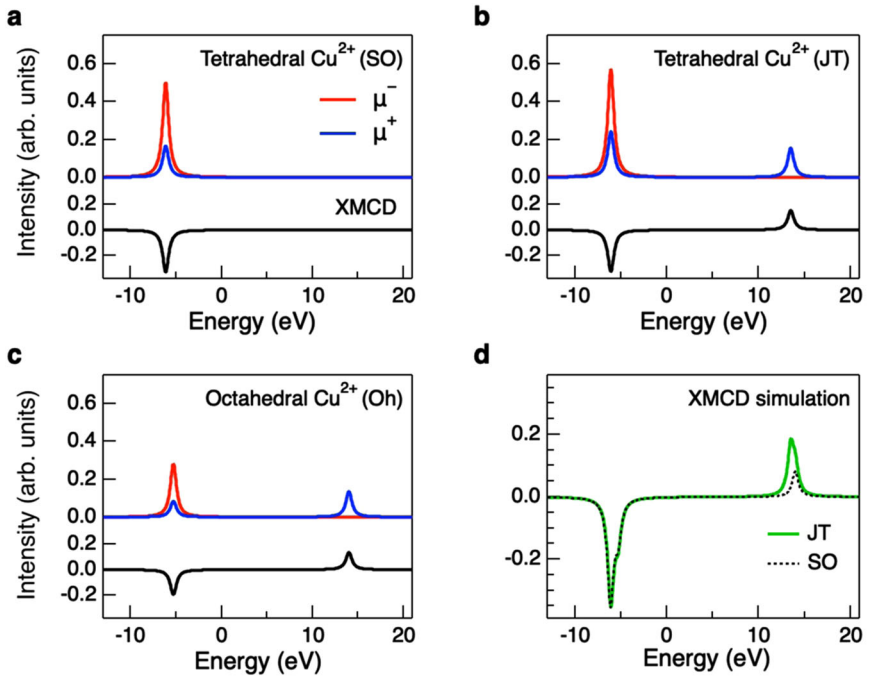

Fig. 4 Simulation of Cu *L*-edge XMCD. a–c The calculated XAS and XMCD spectra of Cu^{2+} tetrahedron in the spin-orbit coupling (SO) scheme, Cu^{2+} tetrahedron in the Jahn-Teller (JT) coupling scheme and Cu^{2+} octahedron, respectively. The calculations are down with an external magnetic field 1 T alone the z direction, and the polarization of incident X-ray lies on the xy plane. **d** The thick green line is the calculated XMCD spectra from 37.5% O_h Cu^{2+} and 62.5% T_d Cu^{2+} with Jahn-Teller distortion; the dashed black line is the result of 37.5% O_h Cu^{2+} and 62.5% spin-orbital entangled T_d Cu^{2+}.

separate the contribution of octahedral Cu^{2+} to the L_2 absorption from that of tetrahedral sites by examining the incident-energy dependence of Cu L_2-edge RIXS.

Resonant inelastic X-ray scattering

RIXS has been proved to be a powerful probe of crystal-field excitation from different site symmetry[27]. By selecting the incident photon to particular absorption energy, RIXS measures electronic excitations of *d* electrons with the site-specific orbital degree of freedom. Figure 2(b),(c) show the RIXS intensity maps of $CuAl_2O_4$ measured about Cu L_3 and L_2 edges, respectively. The scattering angle was fixed at 90°. The L_3-edge RIXS map shows two sets of distinct excitation structures which resonate at incident energies of 930 eV and 930.8 eV, respectively, indicating that these

excitations arise from two Cu sites with different crystal field symmetries. Two excitations with energy loss centered at 0.3 eV and 0.82 eV were observed at the first excitation energy, resulting from the *dd* excitations of tetrahedral Cu^{2+}. The excitation at the other incident energy shows only one broad peak at 1.52 eV and is best explained as the *dd* excitations of octahedral Cu^{2+}. Interestingly, similar features occur at Cu L_2-edge RIXS map as well. The Cu L_2-edge RIXS intensity map displays two sets of excitations at incident energies of 949.6 eV and 950.2 eV, respectively. These experimental observations indicate that the Cu L_2-edge XAS spectrum is composed of the $2p-$ to $-3d$ transition of two Cu sites with different crystal field symmetries, like those in the Cu L_3-edge XAS spectrum.

To understand the electronic structure of $CuAl_2O_4$, we analyzed RIXS data through crystal-field multiplet calculations. The RIXS spectra measured at the L_3 resonance energy of T_d Cu^{2+}, i.e., 930 eV, were compared with the atomic multiplet calculations of a single Cu^{2+} ion in the crystal field produced by four ligands O^{2-}, as shown in Fig. 3(a). With the Hartree–Fock value of 3*d* SOC and a 30% reduction in Slater integrals, the calculations explain measured RIXS features well. The RIXS *dd* excitations of tetrahedral Cu^{2+} are mainly composed of the hole transitions within the t_2 states and those from the t_2 to the *e* states. The corresponding RIXS peaks are labeled A and B, respectively. The value of $10Dq$ determines the energy position of peak B, while the value of the Jahn-Teller splitting Δe controls the spectral line shape of B, as shown in Supplementary Fig. 3(a),(b). Similarly, Supplementary Fig. 3(c) shows that the Jahn-Teller splitting Δt_2 dictates the energy position of peak A. Through the comparison of the RIXS data with calculations, we found that the crystal field parameters are: $10Dq = -0.72 \pm 0.05$ eV, $\Delta e = 50 \pm 20$ meV, and $\Delta t_2 = 270 \pm 50$ meV. The CuO_4 tetrahedron was found to be slightly compressed along the *z* axis, lifting the orbital degeneracy of d_{xy}, d_{yz}, d_{zx} states. The Cu L_3-edge RIXS spectra provide explicit spectroscopy evidence for the local distortion in $CuAl_2O_4$. Furthermore, the calculated RIXS intensity at the L_2 edge nearly vanishes when no local distortion was included (dashed gray curves), in contrast to the calculations with CuO_4 structural distortions (black curves). On the other hand, the RIXS spectra measured at the resonance of O_h Cu *L*-edge show only a single structure, indicating a small distortion in the Cu^{2+} octahedron. The calculated RIXS spectra of O_h Cu sites with $10Dq = 1.6$ eV reproduce the experimental data measured at 930.8 eV and 950.2 eV (Fig. 3(b)).

Our results indicate that in $CuAl_2O_4$, an expected spin-orbit Mott insulator, the T_d Cu site is locally compressed. Through comparing the measured RIXS intensities with calculations of compressed CuO_4 tetrahedron and CuO_6 octahedron, we obtained an amount of site disorder 37.5%, in line with the value obtained from diffraction results. These results indicate that the spin-orbital entangled ground state is destabilized against the Jahn-Teller distorted ground state. From a general perspective, when we start from $S = 1/2$ and increase the SOC strength, the $J_{eff} = 1/2$ state admixes only perturbatively. And then at some critical SOC, we have a drastic transition to $J_{eff} = 1/2$, see Fig. 6 in Ref. [28]. Thus, at small SOC as in Cu, one would expect a small admixture of $J_{eff} = 1/2$, to the ground state. In fact, the distorted ground state from our simulations based on RIXS data has 92% overlap with the d_{xy} orbital expected for the JT ground state. In addition, one can measure spectra of X-ray magnetic circular dichroism (XMCD) in Cu *L*-edge absorption to further examine the Jahn-Teller distorted ground state of $CuAl_2O_4$ by applying a high magnetic field. Figure 4 plots XMCD spectra simulated by using the electronic parameters from RIXS. Clearly, the XMCD spectral line shape at the L_2-edge of the $J_{eff} = 1/2$ is significantly different from that of the Jahn-Teller state, as shown in Fig. 4(d). Also, the orbital moment the Jahn-Teller state is expected to be quenched; a future XMCD experimental study will be helpful for further clarification.

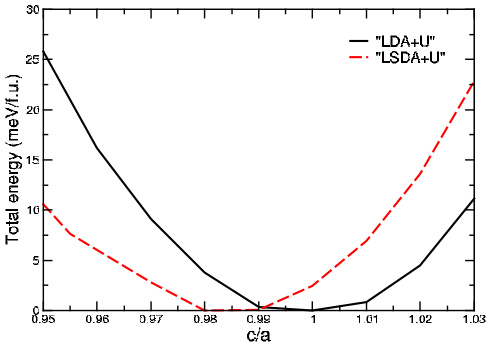

Fig. 5 Total energies as obtained in DFT + *U* + SOC with two different implementations of the + *U* term (black curve - spin-polarization is allowed only in "*U*" part, so-called LDA + U; red - spin polarization is possible in both DFT and "*U*" parts, LSDA + *U*). Minimum at $c/a = 1$ corresponds to SOC $J_{eff} = 1/2$ state, while at $c/a < 1$ to Jahn-Teller $S = 1/2$. These results illustrate that the type of ground state strongly depends on the details of the DFT calculations.

The conclusion drawn from the RIXS data does not disagree with density functional theory (DFT) results of Ref. [15]. It is shown in Ref. [15] that $J_{eff} = 1/2$ state can be realized in a narrow range of parameters used in the calculations. For example, the ground state changes if we change Hubbard *U*. Moreover, our calculations show that the choice of double counting also changes the ground state wavefunction. Figure 5 demonstrates that even the choice of DFT +*U*+SOC calculation scheme may affect the result. Only a delicate balance between Coulomb interaction and SOC stabilizes the $J_{eff} = 1/2$ state, and our *experimental* result shows that most probably this idealized situation is not realized in $CuAl_2O_4$.

DISCUSSION

The spin-orbit materials have become an important class of systems demonstrating exceptional physical properties defined by competition of various interactions such as strong electronic correlations, vibronic and SOCs, etc. Experimental diagnosis of their ground state is a challenging task, which, however, unravels mechanisms lying behind the physical effects observed in these materials. Using RIXS and crystal-field multiplet calculations, we demonstrate that this method is an effective probe of the spin-orbital entangled $J_{eff} = 1/2$ state in 3*d* transition-metal oxides. Being applied to spin-orbit candidate material $CuAl_2O_4$ it shows that, contrary to previous expectations, a competing Jahn-Teller configuration is stabilized in this material, and the tetragonal splittings of the *e* and t_2 orbitals are $\Delta e = 50$ meV and $\Delta t_2 = 270$ meV, respectively. These results suggest that the T_d Cu site is locally compressed. Neither neutron powder diffraction[23] nor single-crystal X-ray diffraction[29] studies observed anomalous atomic displacement in $CuAl_2O_4$, but total scattering measurements like pair-distribution-function analysis will be an excellent probe to study the local structure.

METHODS

Sample synthesis

A stoichiometric mixture of Al_2O_3 (99.9%) and CuO (99.9%) was used for the synthesis of $CuAl_2O_4$. The mixture was pressed into a pellet and then annealed at 1193 K for 84 h and 1293 K for 38 h (with several intermediate grindings) in the air on a Pt foil. X-ray powder diffraction data were measured at room temperature on a RIGAKU MiniFlex600 diffractometer using Cu K*α* radiation (2θ range of 8–140°, a step width of 0.02°, and a scan speed of 1 deg/min). The X-ray data were analyzed by the Rietveld method using RIETAN-2000[30]. The sample was single-phase with sharp reflections. The distribution of Cu^{2+} cations between the tetrahedral 8*a* site and

octahedral 16*d* site was refined with a constraint on the total chemical composition. The experimental, calculated, and difference X-ray diffraction profiles and the main refinement results are shown in Supplementary Fig. 1.

XAS and RIXS measurements

All XAS and RIXS measurements were performed at the AGM-AGS spectrometer of beamline 41A at Taiwan Photon Source[31]. This AGM-AGS beamline is based on the energy compensation principle of grating dispersion. The energy bandwidth of incident X-ray was 314.5 meV while keeping the total energy resolution of RIXS at 90 meV. The sample was at room temperature during the measurements. Both XAS and RIXS measurements were carried out using a linear horizontally (π) polarized X-ray. The XAS spectrum was measured with a normal-incident X-ray in the total electron yield mode. For the RIXS measurement, the incidence angle was 45°, and the scattering angle was fixed at 90°.

Multiplet calculations

Simulations of RIXS, XAS, and XMCD spectra were performed with the full multiplet code through QUANTY, a script language to calculate many-body eigenenergy, XAS, and RIXS spectra[32,33]. The on-site Coulomb interaction, the crystal field, and the 2*p* and 3*d* SOC (ζ_{2p} & ζ_{3d}) were included in the calculations. The intra-atomic Coulomb interaction of 3*d* electrons is described by the radial part of the direct Coulomb interactions $F^2(3d, 3d)$ and $F^4(3d, 3d)$. The interaction between core-hole and 3*d* electrons is described by $F^2(2p, 3d)$ and exchange interactions $G^1(2p, 3d)$, $G^3(2p, 3d)$. The Hartree–Fock values of ζ_{2p} (13.498 eV) and ζ_{3d} (0.102 eV), and a scaling factor 70% for Slater integrals were used in the calculations. The calculations of tetrahedral and octahedral Cu^{2+} were conducted separately with crystal field of −0.72 eV and 1.55 eV, respectively. The calculation of RIXS and XAS spectra are an average of three possible geometries as described in Supplementary Fig. 2.

DFT calculations

DFT calculations were performed using VASP package[34] and PBE type of the exchange-correlation functional[35]. We used 125 k-points for the Brillouin zone integration and chose *U* correction according to ref. [36] with Hubbard $U = 7$ eV[37,38] and Hund's exchange $J_H = 1$ eV.

DATA AVAILABILITY

All data generated or analyzed during this study are available from the corresponding authors upon reasonable request.

Received: 6 September 2021; Accepted: 22 January 2022;
Published online: 21 March 2022

REFERENCES

1. Jackeli, G. & Khaliullin, G. Mott insulators in the strong spin-orbit coupling limit: from Heisenberg to a quantum compass and Kitaev models. *Phys. Rev. Lett.* **102**, 017205 (2009).
2. Pesin, D. & Balents, L. Mott physics and band topology in materials with strong spin–orbit interaction. *Nat. Phys.* **6**, 376–381 (2010).
3. Armitage, N. P., Mele, E. J. & Vishwanath, A. Weyl and Dirac semimetals in three-dimensional solids. *Rev. Mod. Phys.* **90**, 15001 (2018).
4. Takagi, H., Takayama, T., Jackeli, G., Khaliullin, G. & Nagler, S. E. Concept and realization of Kitaev quantum spin liquids. *Nat. Rev. Phys.* **1**, 264–280 (2019).
5. Khomskii, D. I. & Streltsov, S. V. Orbital effects in solids: basics, recent progress, and opportunities. *Chem. Rev.* **121**, 2992 (2021).
6. Rau, J. G., Lee, E. K.-H. & Kee, H.-Y. Spin-orbit physics giving rise to novel phases in correlated systems: Iridates and related materials. *Annu. Rev. Condens. Matter Phys.* **7**, 195–221 (2016).
7. Winter, S. M. et al. Models and materials for generalized Kitaev magnetism. *J. Phys. Condens. Matter* **29**, 493002 (2017).
8. Liu, H. & Khaliullin, G. Pseudospin exchange interactions in d^7 cobalt compounds: Possible realization of the Kitaev model. *Phys. Rev. B* **97**, 014407 (2018).
9. Liu, H., Chaloupka, J. c. v. & Khaliullin, G. Kitaev spin liquid in 3*d* transition metal compounds. *Phys. Rev. Lett.* **125**, 047201 (2020).
10. Zhong, R., Gao, T., Ong, N. P. & Cava, R. J. Weak-field induced nonmagnetic state in a Co-based honeycomb. *Sci. Adv.* **6**, eaay6953 (2020).
11. Kim, C. et al. Antiferromagnetic Kitaev interaction in $J_{\rm eff} = 1/2$ cobalt honeycomb materials $Na_3Co_2SbO_6$ and $Na_2Co_2TeO_6$ (2021).
12. Chen, W. et al. Spin-orbit phase behavior of $Na_2Co_2TeO_6$ at low temperatures. *Phys. Rev. B* **103**, L180404 (2021).
13. Gillig, M. et al. Unusual heat transport of the Kitaev material $Na_2Co_2TeO_6$: putative quantum spin liquid and low-energy spin excitations. J. Phys.: Condens. Matter **34**, 045802 https://arxiv.org/abs/2101.12199 (2022).
14. Nikolaev, S. A., Solovyev, I. V., Ignatenko, A. N., Irkhin, V. Y. & Streltsov, S. V. Realization of the anisotropic compass model on the diamond lattice of Cu^{2+} in $CuAl_2O_4$. *Phys. Rev. B* **98**, 201106 (2018).
15. Kim, C. H. et al. Theoretical evidence of spin-orbital-entangled $J_{\rm eff} = 1/2$ state in the 3*d* transition metal oxide $CuAl_2O_4$. *Phys. Rev. B* **100**, 161104 (2019).
16. Halász, G. B., Perkins, N. B. & van den Brink, J. Resonant inelastic X-ray scattering response of the Kitaev honeycomb model. *Phys. Rev. Lett.* **117**, 127203 (2016).
17. Halász, G. B., Kourtis, S., Knolle, J. & Perkins, N. B. Observing spin fractionalization in the Kitaev spin liquid via temperature evolution of indirect resonant inelastic X-ray scattering. *Phys. Rev. B* **99**, 184417 (2019).
18. Revelli, A. et al. Fingerprints of Kitaev physics in the magnetic excitations of honeycomb iridates. *Phys. Rev. Res.* **2**, 043094 (2020).
19. Lebert, B. W. et al. Resonant inelastic X-ray scattering study of $\alpha - RuCl_3$: a progress report. *J. Condens. Matter Phys.* **32**, 144001 (2020).
20. Suzuki, H. et al. Proximate ferromagnetic state in the Kitaev model material $\alpha - RuCl_3$. *Nat. Commun.* **12**, 4512 (2021).
21. Liu, G.-Q., Antonov, V. N., Jepsen, O. & Andersen., O. K. Coulomb-enhanced spin-orbit splitting: The missing piece in the Sr_2RhO_4 puzzle. *Phys. Rev. Lett.* **101**, 026408 (2008).
22. Cho, H. et al. Pressure-induced transition from $J_{\rm eff} = 1/2$ to $s = 1/2$ states in $CuAl_2O_4$. *Phys. Rev. B* **103**, L081101 (2021).
23. Nirmala, R. et al. Spin glass behavior in frustrated quantum spin system $CuAl_2O_4$ with a possible orbital liquid state. *J. Condens. Matter Phys.* **29**, 13LT01 (2017).
24. Cho, H. et al. Dynamic spin fluctuations in the frustrated *a*-site spinel $CuAl_2O_4$. *Phys. Rev. B* **102**, 014439 (2020).
25. Thole, B. T. & van der Laan, G. Linear relation between X-ray absorption branching ratio and valence-band spin-orbit expectation value. *Phys. Rev. A* **38**, 1943–1947 (1988).
26. Clancy, J. P. et al. Spin-orbit coupling in iridium-based 5*d* compounds probed by X-ray absorption spectroscopy. *Phys. Rev. B* **86**, 195131 (2012).
27. Huang, H. Y. et al. Jahn-Teller distortion driven magnetic polarons in magnetite. *Nat. Commun.* **8**, 15929 (2017).
28. Streltsov, S. V. & Khomskii, D. I. Jahn-Teller effect and spin-orbit coupling: friends or foes? *Phys. Rev. X* **10**, 031043 (2020).
29. Fregola, R. A., Bosi, F., Skogby, H. & Hålenius, U. Cation ordering over short-range and long-range scales in the $MgAl_2O_4$-$CuAl_2O_4$ series. *Am. Mineral.* **97**, 1821–1827 (2012).
30. Izumi, F. & Ikeda, T. A rietveld-analysis programm RIETAN-98 and its applications to zeolites. *Mater. Sci. Forum* **321–324**, 198–205 (2000).
31. Singh, A. et al. Development of the soft X-ray AGM–AGS RIXS beamline at the Taiwan photon source. *J. Synchrotron Radiat.* **28**, 977–986 (2021).
32. Haverkort, M. W., Zwierzycki, M. & Andersen, O. K. Multiplet ligand-field theory using Wannier orbitals. *Phys. Rev. B* **85**, 165113 (2012).
33. Haverkort, M. W. Quanty for core level spectroscopy - excitons, resonances and band excitations in time and frequency domain. *J. Phys. Conf. Ser.* **712**, 012001 (2016).
34. Kresse, G. & Furthmüller, J. Efficient iterative schemes for ab initio total-energy calculations using a plane-wave basis set. *Phys. Rev. B* **54**, 11169–11186 (1996).
35. Perdew, J. P., Burke, K. & Ernzerhof, M. Generalized gradient approximation made simple. *Phys. Rev. Lett.* **77**, 3865–3868 (1996).
36. Liechtenstein, A. I., Anisimov, V. I. & Zaanen, J. Density-functional theory and strong interactions: Orbital ordering in Mott-Hubbard insulators. *Phys. Rev. B* **52**, R5467–R5470 (1995).
37. Markina, M. M. et al. Magnetic phase diagram and first-principles study of $Pb_3TeCo_3V_2O_{14}$. *Phys. Rev. B* **89**, 104409 (2014).
38. Zvereva, E. A. et al. Orbitally induced hierarchy of exchange interactions in zigzag antiferromagnetic state of honeycomb silver delafossite $Ag_3Co_2SbO_6$. *Dalton Trans.* **45**, 7373–7384 (2016).

ACKNOWLEDGEMENTS

This work was supported in part by the Ministry of Science and Technology of Taiwan under Grant No. 109-2112-M-213-010-MY3 and 109-2923-M-213-001. S.V.S. and A.F. acknowledge the support of DFT calculations and theoretical analysis by the Russian Science Foundation via project 20-62-46047. E.K. thanks program AAAA-A18-118020190095-4 (Quantum) of the Russian ministry of science and education. This work was also supported by KAKENHI Grant No. 19K03741 from JSPS, and Program

for Promoting Researches on the Supercomputer Fugaku (Basic Science for Emergence and Functionality in Quantum Matter) from MEXT.

AUTHOR CONTRIBUTIONS

D.J.H. and S.V.S. conceived and coordinated the project. H.Y.H., A.S., C.I.W., C.D.X. J.O., D.J.H., and C.T.C. developed the RIXS instruments and conducted the RIXS experiments. A.A.B. and E.K. synthesized and characterized the sample. H.Y.H. and D.J.H. performed multiplet, and S.V.S. performed DFT calculations. H.Y.H., D.J.H., S.V.S., and A.F. analyzed the data and wrote the paper with inputs from other authors.

COMPETING INTERESTS

The authors declare no competing interests.

ADDITIONAL INFORMATION

Supplementary information The online version contains supplementary material available at https://doi.org/10.1038/s41535-022-00430-0.

Correspondence and requests for materials should be addressed to S. V. Streltsov or D. J. Huang.